Chapter 11

Numerical Analysis of the Incompressible Fluid Flow and Heat Transfer

Toshio Tagawa

Additional information is available at the end of the chapter

http://dx.doi.org/10.5772/intechopen.72263

Abstract

The present chapter introduces incompressible Newtonian fluid flow and heat transfer by using the finite difference method. Since the solution of the Navier-Stokes equation is not simple because of its unsteady and multi-dimensional characteristic, the present chapter focuses on the simplified flows owing to the similarity or periodicity. As a first section, the first Stoke problem is considered numerically by introducing the finite difference method. In the second section, natural convection heat transfer heated from a vertical plate with uniform heat flux is introduced together with the method how to obtain the system of ordinary differential equations. In the third example, linear stability analysis for the onset of secondary flow during the Taylor-Couette flow is numerically treated using the HSMAC method.

Keywords: finite difference method, similar solution, boundary layer, linear stability analysis, HSMAC method

1. Introduction

The governing equation for the fluid flow is known as Navier-Stokes equation, which is however difficult to solve analytically; and therefore, a lot of numerical techniques have been proposed and developed. Nevertheless various complex flow phenomena such as turbulent flow, multi-phase flow, compressible flow, combustion, and phase change encountered in the fields of engineering would have still difficulties to circumvent even using both present computational resources and numerical techniques. The present chapter devotes not to elucidate such complex phenomena, but to introduce rather simplified fluid flow by using the finite difference method.

One focuses on incompressible flows, in which physical properties such as the viscosity, the thermal conductivity, the specific heat are constant and even the fluid density is not a thermodynamic variable. This simplified assumption makes the fluid flow phenomena much easier to

be handled and it is valid when the flow velocity is much slower than the sound velocity and/or the temperature difference in the fluid is small enough to consider the thermal expansion coefficient is independent to the temperature. The former situation is known the *low Mach number approximation*, while the latter one the *Boussinesq approximation*.

Another simplification on the incompressible flows is the reduction of dimension due to the characteristic of similarity and periodicity. For the boundary layer flows such as the *Blasius flow*, the *stagnation-point flow*, and the *von Kármán rotating disk flow* have the similar solution where the flow transition from laminar to turbulence does not occur. In those cases, a combined dimensionless variable (similar variable) η is introduced and the velocity distribution can be only a function of η. While for the onset of instability such as the *Rayleigh-Bénard convection*, the *Bénard-Marangoni convection*, and the *Taylor-Couette flow*, the periodic characteristic of flow structure is observed. At the stage of onset of instability, the non-linear term is negligible and therefore the function of flow field is separated into the amplitude part and periodic part, respectively. This makes the effort on numerical analysis to reduce significantly and also to contribute the augmentation of accuracy of the results.

This chapter consists of three main bodies. First, a numerical technique for solving the boundary value problem called the *first Stokes problem* or the *Rayleigh problem* [1] is introduced. The differential equation is transferred into an ordinary equation and it is solved by a finite difference method using the Jacobi method. Second, similar solution of natural convection heat transfer heated from a vertical plate with uniform heat flux is introduced together with the method how to obtain the system of ordinary differential equations. The obtained Nusselt numbers are compared with some previous studies. Third, for example, of the linear stability analysis, one shows that the HSMAC method can be applied to obtain the critical values for the onset of secondary flow such as the *Taylor-Couette flow*. The Eigen functions of flow and pressure fields are visualized.

2. Unsteady flow due to sudden movement of the plate

2.1. Governing equations

An infinite length plate is set in a stationary fluid as an initial condition. Let us consider the situation that the infinite length plate suddenly moves along its parallel direction at a constant speed u_w. This problem was first solved by Stokes [2] in his famous treatment of the pendulum. Since Lord Rayleigh [3] also treated this flow, it is often called the *Rayleigh problem* in the literature. One takes that x is the plate movement direction and y is distance from the plate. Since the velocity component perpendicular to the plate v is zero, the momentum equation is simplified and is shown as a diffusion equation

$$\frac{\partial u}{\partial t} = \nu \frac{\partial^2 u}{\partial y^2} \tag{1}$$

Here, u is the velocity component parallel to the plate direction, t is the time, and ν is the kinematic viscosity. The boundary conditions for this partial differential equation are as follows:

http://dx.doi.org/10.5772/intechopen.72263

$$\begin{cases} y = 0: & u = u_w \\ y \to \infty: & u \to 0 \end{cases} \tag{2}$$

In order to reduce the partial differential equation to an ordinary equation, the following dimensionless velocity U and the similar variable η are introduced

$$u = u_w U(\eta), \quad \eta = \frac{y}{2\sqrt{\nu t}} \tag{3}$$

Then, the following ordinary differential equation can be obtained

$$\frac{d^2U}{d\eta^2} + 2\eta \frac{dU}{d\eta} = 0 \tag{4}$$

The boundary condition for the ordinary differential equation is as follows using the similar variable η instead of y:

$$\begin{cases} \eta = 0: & U = 1 \\ \eta \to \infty: & U \to 0 \end{cases} \tag{5}$$

As a consequence, one needs to solve this boundary value problem. The theoretical solution can be easily obtained and expressed using the error function

$$U = \frac{u}{u_w} = 1 - \text{erf}(\eta) = 1 - \frac{2}{\sqrt{\pi}} \int_0^\eta \exp\left(-\xi^2\right) d\xi \tag{6}$$

The velocity profile is shown in **Figure 1**.

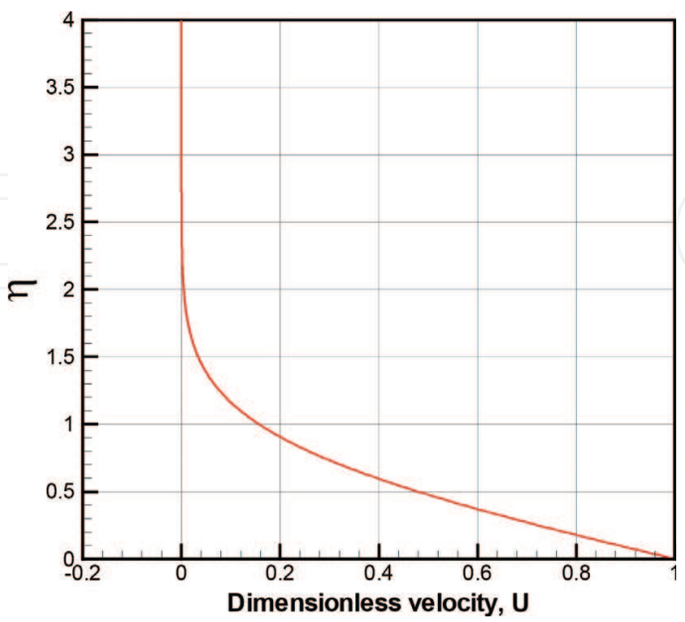

Figure 1. Velocity profile.

2.2. Numerical method for solving the ordinary differential equation using finite difference method

For numerical solution, it is necessary to define the range of η, as recognized from **Figure 1**, $\eta = 4$ is enough. Hence, the boundary condition shown below is used instead of Eq. (5)

$$\begin{cases} \eta = 0: & U = 1 \\ \eta = 4: & U = 0 \end{cases} \tag{7}$$

As illustrated in **Figure 2**, in which vertical and horizontal axes are exchanged from **Figure 1**, one needs to obtain each value of dimensionless velocity numerically. The approximated velocity profile is expressed by connecting these values smoothly. For simplicity, the intervals between neighboring two points are the same and it is noted as $\Delta\eta$. When the second-order central difference method is used, Eq. (4) is as follows:

$$\frac{U_{i+1} - 2U_i + U_{i-1}}{(\Delta\eta)^2} + 2\eta_i \frac{U_{i+1} - U_{i-1}}{2(\Delta\eta)} = 0, \quad (i = 2, 3, \cdots N-1)$$

Here, N is total number of grids and in this chapter, the first grid point starts from 1 as its definition. The above equation becomes

$$\underbrace{\{1 - \eta_i(\Delta\eta)\}}_{\alpha_i} U_{i-1} - 2U_i + \underbrace{\{1 + \eta_i(\Delta\eta)\}}_{\beta_i} U_{i+1} = 0, \quad (i = 2, 3, \cdots N-1). \tag{8}$$

Here, $\eta_i = (i-1)(\Delta\eta)$ and α_i and β_i are coefficients determined by the number of grids. The boundary condition (7) is modified

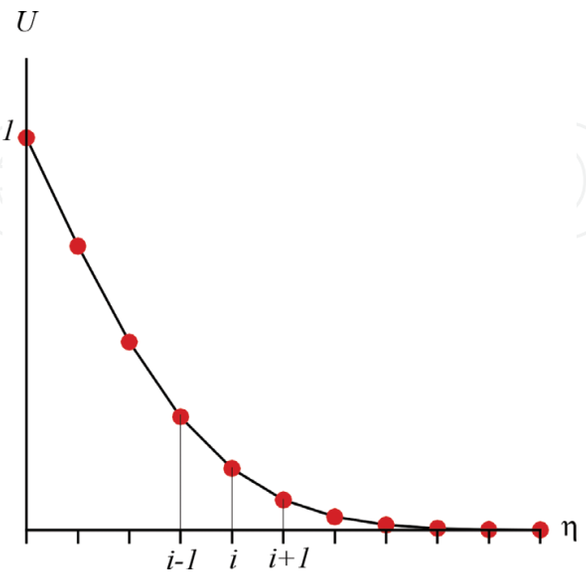

Figure 2. Equidistant grids discretized.

http://dx.doi.org/10.5772/intechopen.72263

$$\begin{cases} \eta = 0: & U_1 = 1 \\ \eta = 4: & U_N = 0 \end{cases} \tag{9}$$

In the following, the case of $N = 7$ is considered, for example. By substituting $i = 2$–6 into Eq. (8), the following simultaneous equation is obtained:

$$\begin{pmatrix} -2 & \beta_2 & 0 & 0 & 0 \\ \alpha_3 & -2 & \beta_3 & 0 & 0 \\ 0 & \alpha_4 & -2 & \beta_4 & 0 \\ 0 & 0 & \alpha_5 & -2 & \beta_5 \\ 0 & 0 & 0 & \alpha_6 & -2 \end{pmatrix} \begin{pmatrix} U_2 \\ U_3 \\ U_4 \\ U_5 \\ U_6 \end{pmatrix} = \begin{pmatrix} -\alpha_2 U_1 \\ 0 \\ 0 \\ 0 \\ -\beta_6 U_7 \end{pmatrix} \tag{10}$$

This kind of tridiagonal matrix is often seen and can be solved by a direct numerical method, such as Tomas method. However, the rank of the matrix is usually extremely large and one introduces an iterative method for solving the king-size matrix.

2.3. Iterative method for matrix solver

In general, the rank of the matrix appearing in computational fluid dynamics (CFD) is large and iterative methods such as Jacobi, Gauss-Seidel, or successive over relaxation (SOR) methodare employed. In this subsection, the Jacobi method is explained. The matrix can be divided into three parts of lower, diagonal, and upper as follows:

$$\begin{pmatrix} 0 & 0 & 0 & 0 & 0 \\ \alpha_3 & 0 & 0 & 0 & 0 \\ 0 & \alpha_4 & 0 & 0 & 0 \\ 0 & 0 & \alpha_5 & 0 & 0 \\ 0 & 0 & 0 & \alpha_6 & 0 \end{pmatrix} \begin{pmatrix} U_2 \\ U_3 \\ U_4 \\ U_5 \\ U_6 \end{pmatrix} + \begin{pmatrix} -2 & 0 & 0 & 0 & 0 \\ 0 & -2 & 0 & 0 & 0 \\ 0 & 0 & -2 & 0 & 0 \\ 0 & 0 & 0 & -2 & 0 \\ 0 & 0 & 0 & 0 & -2 \end{pmatrix} \begin{pmatrix} U_2 \\ U_3 \\ U_4 \\ U_5 \\ U_6 \end{pmatrix}$$
$$+ \begin{pmatrix} 0 & \beta_2 & 0 & 0 & 0 \\ 0 & 0 & \beta_3 & 0 & 0 \\ 0 & 0 & 0 & \beta_4 & 0 \\ 0 & 0 & 0 & 0 & \beta_5 \\ 0 & 0 & 0 & 0 & 0 \end{pmatrix} \begin{pmatrix} U_2 \\ U_3 \\ U_4 \\ U_5 \\ U_6 \end{pmatrix} = \begin{pmatrix} -\alpha_2 U_1 \\ 0 \\ 0 \\ 0 \\ -\beta_{N-1} U_N \end{pmatrix} \tag{11}$$

In the Jacobi method, only the diagonal part is put in the left-hand side ($n + 1$ step), while the lower and upper parts are moved to the right-hand side (n step)

$$\underbrace{\begin{pmatrix} -2 & 0 & 0 & 0 & 0 \\ 0 & -2 & 0 & 0 & 0 \\ 0 & 0 & -2 & 0 & 0 \\ 0 & 0 & 0 & -2 & 0 \\ 0 & 0 & 0 & 0 & -2 \end{pmatrix}}_{D} \underbrace{\begin{pmatrix} U_2 \\ U_3 \\ U_4 \\ U_5 \\ U_6 \end{pmatrix}^{n+1}}_{\vec{U}n+1} = \underbrace{\begin{pmatrix} -\alpha_2 U_1 \\ 0 \\ 0 \\ 0 \\ -\beta_{N-1} U_N \end{pmatrix}}_{\vec{b}} - \underbrace{\begin{pmatrix} 0 & 0 & 0 & 0 & 0 \\ \alpha_3 & 0 & 0 & 0 & 0 \\ 0 & \alpha_4 & 0 & 0 & 0 \\ 0 & 0 & \alpha_5 & 0 & 0 \\ 0 & 0 & 0 & \alpha_6 & 0 \end{pmatrix}}_{L} \underbrace{\begin{pmatrix} U_2 \\ U_3 \\ U_4 \\ U_5 \\ U_6 \end{pmatrix}^{n}}_{\vec{U}n}$$

$$- \underbrace{\begin{pmatrix} 0 & \beta_2 & 0 & 0 & 0 \\ 0 & 0 & \beta_3 & 0 & 0 \\ 0 & 0 & 0 & \beta_4 & 0 \\ 0 & 0 & 0 & 0 & \beta_5 \\ 0 & 0 & 0 & 0 & 0 \end{pmatrix}}_{U} \underbrace{\begin{pmatrix} U_2 \\ U_3 \\ U_4 \\ U_5 \\ U_6 \end{pmatrix}^{n}}_{\vec{U}n} \quad (12)$$

Here, n is the old iteration step and $n + 1$ is the new iteration step. Hence, the following equation is repeatedly used:

$$\vec{U}^{n+1} = D^{-1}\left[\vec{b} - (L+U)\vec{U}^{n}\right] \quad (13)$$

This is equivalent to the following equation:

$$U_i^{n+1} = \frac{1}{2}\left(\alpha_i U_{i-1}^{n} + \beta_i U_{i+1}^{n}\right), \quad (i = 2,3,4,5,6) \quad (14)$$

By using Eq. (9), Eq. (14) is computed repeatedly and then the value of each grid gradually converges to a certain solution. The Gauss-Seidel and SOR methods are known as the faster convergence method.

3. Similarity solution for natural convection heated from a vertical plate

3.1. Introduction

In this section, let us consider the natural convection heat transfer for a vertical plate heated with uniform heat flux in the wide range of Prandtl number from zero to infinity. In order to explain the numerical method as how to solve the governing equations, one assumes that the flow and temperature fields formed in the vicinity of the heated plate have a similarity and then one introduces the finite difference method to obtain numerical results.

3.2. Governing equations

One assumes that the flow is incompressible laminar and boundary layer equations are used in this analysis. The governing equations with presuming the Boussinesq approximation are

shown in Eqs. (15)–(17) together with the boundary condition (18). Here, one defines that x axis is in the vertical direction and its velocity component is u, and y axis is in the direction perpendicular to the vertical plate and its velocity component is v.

Continuity of mass

$$\frac{\partial u}{\partial x}+\frac{\partial v}{\partial y}=0 \tag{15}$$

Momentum equation

$$u\frac{\partial u}{\partial x}+v\frac{\partial u}{\partial y}=\nu\frac{\partial^2 u}{\partial y^2}+g\beta(T-T_\infty) \tag{16}$$

Energy equation

$$u\frac{\partial T}{\partial x}+v\frac{\partial T}{\partial y}=\alpha\frac{\partial^2 T}{\partial y^2} \tag{17}$$

Boundary equation

$$\begin{cases} y=0: & u=v=0, \quad q=-k(\partial T/\partial y) \\ y\to\infty: & u\to 0, \quad T\to T_\infty \end{cases} \tag{18}$$

Here, β is the thermal expansion coefficient, g is the acceleration due to gravity, α is the thermal diffusivity, k is the thermal conductivity, and T is the temperature.

3.3. Non-dimensionalization

First, dimensionless variables, such as velocity and temperature, are set as follows using the unknown reference value denoted with subscripts a and b:

$$X=\frac{x}{x_a}, \quad Y=\frac{y}{y_a}, \quad U=\frac{u}{u_a}, \quad V=\frac{v}{v_a}, \quad \theta=\frac{T-T_b}{T_a} \tag{19}$$

Equation (19) is substituted into Eqs. (15)–(18), and one gets

$$\frac{\partial U}{\partial X}+\underbrace{\frac{v_a x_a}{y_a u_a}}_{[1]}\frac{\partial V}{\partial Y}=0$$

$$U\frac{\partial U}{\partial X}+\underbrace{\frac{v_a x_a}{y_a u_a}}_{[1]}V\frac{\partial U}{\partial Y}=\underbrace{\frac{\nu x_a}{{y_a}^2 u_a}}_{[2]}\frac{\partial^2 U}{\partial Y^2}+\underbrace{\frac{g\beta(T_b-T_\infty)x_a}{{u_a}^2}}_{[3]}+\underbrace{\frac{g\beta T_a x_a}{{u_a}^2}}_{[4]}\theta$$

$$U\frac{\partial\theta}{\partial X}+\underbrace{\frac{v_a x_a}{y_a u_a}}_{[1]}V\frac{\partial\theta}{\partial Y}=\underbrace{\frac{\alpha x_a}{{y_a}^2 u_a}}_{[5]}\frac{\partial^2\theta}{\partial Y^2}$$

$$\begin{cases} Y=0: \quad U=V=0, \quad \underbrace{(qy_a)/(kT_a)}_{[6]}=-\partial\theta/\partial Y \\ Y\to\infty: \quad U=0, \quad \theta=\underbrace{(T_\infty-T_b)/T_a}_{[7]} \end{cases}$$

At the moment stage, x_a is recognized as the height of the vertical plate.

Putting [3] = 0, and one obtains $T_b=T_\infty$.Hence [7] becomes $\theta=0$.

Putting [6] = 1, and one gets $\frac{qy_a}{kT_a}=1 \quad \Rightarrow \quad T_a=\frac{qy_a}{k}$

Putting [5] = 1, and one gets $\frac{\alpha x_a}{{y_a}^2 u_a}=1 \quad \Rightarrow \quad y_a=\left(\frac{\alpha x_a}{u_a}\right)^{1/2}$

Putting [1] = 1, $\frac{v_a x_a}{y_a u_a}=1 \quad \Rightarrow \quad v_a=\frac{y_a u_a}{x_a}$

Putting [4] = 1, $\frac{g\beta T_a x_a}{{u_a}^2}=1 \quad \Rightarrow \quad u_a=\left(g\beta T_a x_a\right)^{1/2}=\left(g\beta\frac{qy_a}{k}x_a\right)^{1/2}=\left(g\beta\frac{q}{k}\left(\frac{\alpha x_a}{u_a}\right)^{1/2}x_a\right)^{1/2}$

$$\therefore \quad u_a=\left\{\left(g\beta\frac{q}{k}\right)^2\alpha{x_a}^3\right\}^{1/5}=\left(\frac{g\beta q{x_a}^4}{k\alpha^2}\right)^{2/5}\frac{\alpha}{x_a}=(Ra^*Pr)^{2/5}\frac{\alpha}{x_a}, \quad \because Ra^*=\frac{g\beta q{x_a}^4}{k\alpha\nu} \tag{20}$$

$$y_a=\left(\frac{\alpha x_a}{u_a}\right)^{1/2}=\left(\frac{\alpha x_a}{(Ra^*Pr)^{2/5}\frac{\alpha}{x_a}}\right)^{1/2}=\left(\frac{{x_a}^2}{(Ra^*Pr)^{2/5}}\right)^{1/2}=x_a(Ra^*Pr)^{-1/5} \tag{21}$$

$$T_a=\frac{qy_a}{k}=\frac{q}{k}\frac{x_a}{(Ra^*Pr)^{1/5}}=\frac{qx_a}{k}(Ra^*Pr)^{-1/5} \tag{22}$$

$$v_a=\frac{y_a u_a}{x_a}=\frac{\frac{x_a}{(Ra^*Pr)^{1/5}}(Ra^*Pr)^{2/5}\frac{\alpha}{x_a}}{x_a}=(Ra^*Pr)^{1/5}\frac{\alpha}{x_a} \tag{23}$$

In the above process, finally one obtains the dimensionless equations as follows:

$$\frac{\partial U}{\partial X}+\frac{\partial V}{\partial Y}=0 \tag{24}$$

$$U\frac{\partial U}{\partial X}+V\frac{\partial U}{\partial Y}=Pr\frac{\partial^2 U}{\partial Y^2}+\theta \tag{25}$$

$$U\frac{\partial\theta}{\partial X}+V\frac{\partial\theta}{\partial Y}=\frac{\partial^2\theta}{\partial Y^2} \tag{26}$$

$$\begin{cases} Y = 0: & U = V = 0, \quad \partial\theta/\partial Y = -1 \\ Y \to \infty: & U = 0, \quad \theta = 0 \end{cases} \tag{27}$$

The dimensionless variables are summarized as follows:

$$\begin{aligned} X &= \frac{x}{x_a}, \quad Y = \frac{y}{x_a (Ra^* Pr)^{-1/5}}, \quad U = \frac{u}{\frac{\alpha}{x_a}(Ra^* Pr)^{2/5}}, \\ V &= \frac{v}{\frac{\alpha}{x_a}(Ra^* Pr)^{1/5}}, \quad \theta = \frac{T - T_\infty}{\frac{qx_a}{k}(Ra^* Pr)^{-1/5}} \end{aligned} \tag{28}$$

Furthermore, one assumes that the velocity and temperature fields has a similarity along the direction of vertical plate, so one puts X = 1. These equations are useful for analyzing low Prandtl number cases and summarized as follows:

Low Prandtl number

Continuity of mass

$$\frac{dV}{d\eta} = \frac{1}{5}\left(\eta \frac{dU}{d\eta} - 3U\right) \tag{29}$$

Momentum equation

$$U\frac{dV}{d\eta} - V\frac{dU}{d\eta} + Pr\frac{d^2U}{d\eta^2} + \theta = 0 \tag{30}$$

Energy equation

$$\frac{U}{5}\left(\eta \frac{d\theta}{d\eta} - \theta\right) - V\frac{d\theta}{d\eta} + \frac{d^2\theta}{d\eta^2} = 0 \tag{31}$$

Boundary conditions

$$\begin{cases} \eta = 0: & U = V = 0, \quad d\theta/d\eta = -1 \\ \eta \to \infty: & U = \theta = 0 \end{cases} \tag{32}$$

The dimensionless variables and non-dimensional numbers are defined as follows:

$$\begin{aligned} \eta &= \frac{y}{x(Ra_x{}^* Pr)^{-\frac{1}{5}}}, \quad U = \frac{u}{\frac{\alpha}{x}(Ra_x{}^* Pr)^{\frac{2}{5}}}, \quad V = \frac{v}{\frac{\alpha}{x}(Ra_x{}^* Pr)^{\frac{1}{5}}}, \\ \theta &= \frac{T - T_\infty}{\frac{qx}{k}(Ra_x{}^* Pr)^{-\frac{1}{5}}}, \quad Ra_x{}^* = \frac{g\beta q x^4}{\alpha \nu k}, \quad Pr = \frac{\nu}{\alpha} \end{aligned} \tag{33}$$

The local Nusselt number can be obtained by the following derivation:

$$Nu_x = \frac{h_x x}{k} = \frac{qx}{(T_w - T_\infty)k} = \frac{qx}{T_a \theta_w k} = \underbrace{\frac{\left(\frac{g\beta q}{\alpha^2 k}\right)^{1/5} k}{qx^{1/5}}}_{T_a{}^{-1}} \frac{qx}{\theta_w k} \tag{34}$$

$$= \left(\frac{g\beta q}{\alpha^2 k}\right)^{1/5} \frac{x^{4/5}}{\theta_w} = \left(\frac{g\beta q x^4}{\alpha^2 k}\right)^{1/5} \frac{1}{\theta_w} = \left(Ra_x^* Pr\right)^{1/5} \frac{1}{\theta_w}$$

$$Nu_x = (Ra_x{}^* Pr)^{\frac{1}{5}} \left(\theta|_{\eta=0}\right)^{-1} = (Ra_x Nu_x Pr)^{\frac{1}{5}} \left(\theta|_{\eta=0}\right)^{-1} \tag{35}$$

Therefore, the local Nusselt number can be obtained just from the dimensionless temperature at the wall using Eq. (36)

$$\frac{Nu_x}{(Ra_x Pr)^{\frac{1}{4}}} = \left(\theta|_{\eta=0}\right)^{-\frac{5}{4}} \tag{36}$$

High Prandtl number

If the Prandtl number is higher than unity, the following equations are useful:

Continuity of mass

$$\frac{dV}{d\eta} = \frac{1}{5}\left(\eta \frac{dU}{d\eta} - 3U\right) \tag{37}$$

Momentum equation

$$U\frac{dV}{d\eta} - V\frac{dU}{d\eta} + Pr\frac{d^2U}{d\eta^2} + Pr\theta = 0 \tag{38}$$

Energy equation

$$\frac{U}{5}\left(\eta \frac{d\theta}{d\eta} - \theta\right) - V\frac{d\theta}{d\eta} + \frac{d^2\theta}{d\eta^2} = 0 \tag{39}$$

Boundary conditions

$$\begin{cases} \eta = 0: & U = V = 0, \quad d\theta/d\eta = -1 \\ \eta \to \infty: & U = \theta = 0 \end{cases} \tag{40}$$

The dimensionless variables and non-dimensional numbers are defined as follows:

$$\eta = \frac{y}{x(Ra_x{}^*)^{-\frac{1}{5}}}, \quad U = \frac{u}{\frac{\alpha}{x}(Ra_x{}^*)^{\frac{2}{5}}}, \quad V = \frac{v}{\frac{\alpha}{x}(Ra_x{}^*)^{\frac{1}{5}}},$$
$$\theta = \frac{T - T_\infty}{\frac{qx}{k}(Ra_x{}^*)^{-\frac{1}{5}}}, \quad Ra_x{}^* = \frac{g\beta q x^4}{\alpha \nu k}, \quad Pr = \frac{\nu}{\alpha} \tag{41}$$

http://dx.doi.org/10.5772/intechopen.72263

$$\frac{Nu_x}{(Ra_x)^{\frac{1}{4}}} = \left(\theta|_{\eta=0}\right)^{-\frac{5}{4}} \tag{42}$$

3.4. Numerical results

Figure 3 shows the numerical result for the various Prandtl number cases. The upper figures indicate the vertical velocity and lower ones the temperature. The left-hand side figures show the cases of $\Pr \geq 1$, while the right-hand side ones the cases of $\Pr \leq 1$

Table 1 shows the summary of the local Nusselt number for various Prandtl number cases together with the reference of Churchill and Ozoe for comparison [4]. The agreement is quite good except for the extreme cases such as $\Pr \to 0$ and ∞. In such extreme cases, a small amount of discrepancy exists. In this study, the boundary condition for $\Pr \to 0$

$$\begin{cases} \eta = 0: & dU/d\eta = V = 0, \quad d\theta/d\eta = -1 \\ \eta \to \infty: & U = \theta = 0 \end{cases}$$

and that for $\Pr \to \infty$

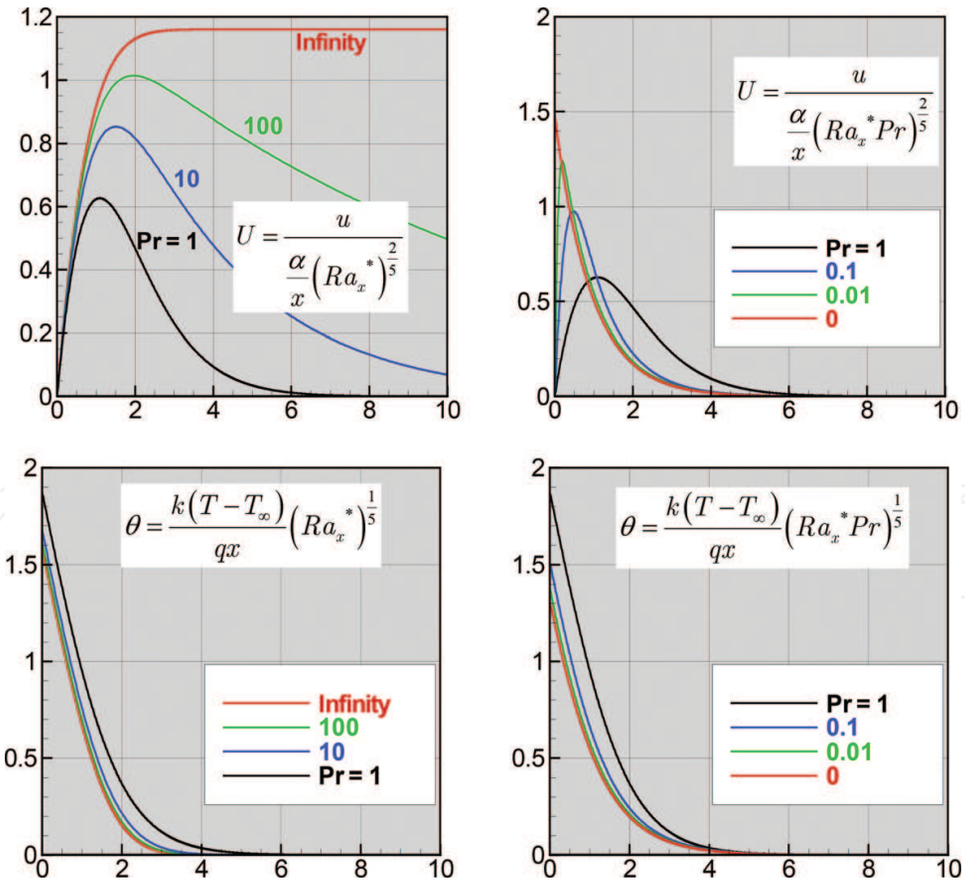

Figure 3. Vertical velocity and temperature distributions for various Prandtl numbers. The left-hand side indicates high Prandtl number cases while the right-hand side low Prandtl number cases.

Pr	0	0.01	0.1	1	10	100	∞
$\frac{Nu_x}{(Ra_x)^{1/4}}$	N/A			0.4564 0.456	0.5234 0.524	0.5495 0.550	0.5631 0.5627
$\frac{Nu_x}{(Ra_x Pr)^{1/4}}$	0.7107 0.6922	0.6694 0.670	0.5970 0.597	0.4564 0.456	N/A		

Table 1. Local Nusselt number for various values of Prandtl number (the upper: present results, the lower: Churchill and Ozoe [4]).

$$\begin{cases} \eta = 0: & U = V = 0, \quad d\theta/d\eta = -1 \\ \eta \to \infty: & dU/d\eta = \theta = 0. \end{cases}$$

are used. Owing to this kind of special treatments for the boundary condition of such extreme cases, one can obtain accurate numerical results for the system of ordinary equations. The results between the solution of the present method and that of Le Fevre [5] for the case of constant temperature of heated wall are identical to each other. The value for Pr → ∞ is 0.5027 and that for Pr = 0 is 0.6004.

4. Linear stability of Taylor-Couette flow

4.1. Governing equations

In the text book of Chandrasekar [6], various examples of the linear stability analysis such as the *Rayleigh-Bénard convection*, the *Taylor-Couette flow*, and the *Rayleigh-Taylor instability* were studied extensively. More recently, Koschmieder [7] described the research focusing on the *Bénard cells* and the *Taylor vortices*. In this section, only the Taylor-Coette flow is considered. **Figure 4** shows the schematic model considered for the Taylor-Couette flow. In this section, the fluid flow inside of the co-axial double cylindrical enclosure is assumed to be incompressible Newtonian, isothermal and axisymmetric. The gray part represents the computational domain. It is known that the stationary secondary flow is generated at a certain condition under the influence of centrifugal force due to the rotation of primary basic flow which is in azimuthal direction. The continuity of mass and momentum equations are shown in the cylindrical coordinate system as follows:

$$\frac{\partial u_r}{\partial r} + \frac{u_r}{r} + \frac{\partial u_z}{\partial z} = 0 \tag{43}$$

$$\frac{\partial u_r}{\partial t} + u_r \frac{\partial u_r}{\partial r} + u_z \frac{\partial u_r}{\partial z} - \frac{{u_\theta}^2}{r} = -\frac{1}{\rho}\frac{\partial p}{\partial r} + \nu\left(\frac{\partial^2 u_r}{\partial r^2} + \frac{1}{r}\frac{\partial u_r}{\partial r} - \frac{u_r}{r^2} + \frac{\partial^2 u_r}{\partial z^2}\right) \tag{44}$$

$$\frac{\partial u_\theta}{\partial t} + u_r \frac{\partial u_\theta}{\partial r} + u_z \frac{\partial u_\theta}{\partial z} + \frac{u_r u_\theta}{r} = \nu\left(\frac{\partial^2 u_\theta}{\partial r^2} + \frac{1}{r}\frac{\partial u_\theta}{\partial r} - \frac{u_\theta}{r^2} + \frac{\partial^2 u_\theta}{\partial z^2}\right) \tag{45}$$

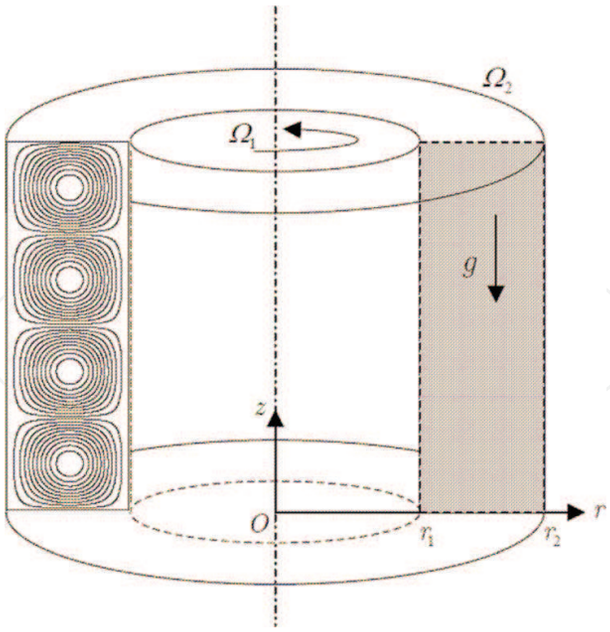

Figure 4. Schematic model for the Taylor-Couette flow.

$$\frac{\partial u_z}{\partial t} + u_r \frac{\partial u_z}{\partial r} + u_z \frac{\partial u_z}{\partial z} = -\frac{1}{\rho}\frac{\partial p}{\partial z} + \nu\left(\frac{\partial^2 u_z}{\partial r^2} + \frac{1}{r}\frac{\partial u_z}{\partial r} + \frac{\partial^2 u_z}{\partial z^2}\right) - g \tag{46}$$

Here, it is indicated that r is the radial, θ is the azimuthal, and z is the axial components.

4.2. Basic state and linearization

The cylindrical enclosure is long enough to neglect the top and bottom ends. In that situation, the basic states for the azimuthal component of velocity and pressure are as follows:

Azimuthal velocity

$$\overline{u}_\theta(r) = -\frac{r_2^2\Omega_2 - r_1^2\Omega_1}{r_1^2 - r_2^2}r + \frac{r_1^2 r_2^2(\Omega_2 - \Omega_1)}{r_1^2 - r_2^2}\frac{1}{r} \tag{47}$$

Pressure

$$\overline{p}(r,z) = \int \frac{\rho\{\overline{u}_\theta(r)\}^2}{r}\ dr - \rho g z + p_0 \tag{48}$$

Here, Ω_1 is the angular velocity at the inner cylinder, Ω_2 is the angular velocity at the outer cylinder, p is the pressure, ρ is the density, and g is the acceleration due to gravity. In order to derive disturbance equations for the linear stability, the three components of velocity and pressure are represented as a summation of basic state and infinitesimal disturbance as follows:

$$u_\theta(r,z,t) = \overline{u}_\theta(r) + v'(r,z,t), \quad u_r(r,z,t) = u'(r,z,t), \quad u_z(r,z,t) = w'(r,z,t), \\ p(r,z,t) = \overline{p}(r,z) + p'(r,z,t) \tag{49}$$

After neglecting the second-order disturbance, the following linearized equations are obtained:

$$\frac{\partial u'}{\partial r} + \frac{u'}{r} + \frac{\partial w'}{\partial z} = 0 \tag{50}$$

$$\frac{\partial u'}{\partial t} = -\frac{1}{\rho}\frac{\partial p'}{\partial r} + \nu\left(\frac{\partial^2 u'}{\partial r^2} + \frac{1}{r}\frac{\partial u'}{\partial r} - \frac{u'}{r^2} + \frac{\partial^2 u'}{\partial z^2}\right) + \frac{2\overline{u}_\theta v'}{r} \tag{51}$$

$$\frac{\partial v'}{\partial t} = \nu\left(\frac{\partial^2 v'}{\partial r^2} + \frac{1}{r}\frac{\partial v'}{\partial r} - \frac{v'}{r^2} + \frac{\partial^2 v'}{\partial z^2}\right) - \left(\frac{d\overline{u}_\theta}{dr} + \frac{\overline{u}_\theta}{r}\right)u' \tag{52}$$

$$\frac{\partial w'}{\partial t} = -\frac{1}{\rho}\frac{\partial p'}{\partial z} + \nu\left(\frac{\partial^2 w'}{\partial r^2} + \frac{1}{r}\frac{\partial w'}{\partial r} + \frac{\partial^2 w'}{\partial z^2}\right) \tag{53}$$

By considering the periodicity of the secondary flow which could be happened, each component of infinitesimal disturbance is assumed to be given in the following form. Here, a is the axial wavenumber (real number) and s is angular frequency (complex number)

$$\frac{u'}{\tilde{u}(r)} = \frac{v'}{\tilde{v}(r)} = \frac{w'}{\tilde{w}(r)} = \frac{p'}{\tilde{p}(r)} = \exp(iaz + st) \tag{54}$$

4.3. Linear stability analysis

The dimensionless simultaneous ordinary equations are summarized as follows:

Basic velocity

$$\overline{U}_\theta(R) = \frac{\mu - \eta^2}{1 - \eta^2}R + \frac{\eta^2(1-\mu)}{1-\eta^2}\frac{1}{R} \tag{55}$$

Disturbance equations for amplitude functions

$$D_*\tilde{U} + ik\tilde{W} = 0 \tag{56}$$

$$S\tilde{U} = -D\tilde{P} + \left(DD_* - k^2\right)\tilde{U} + Re_\Omega\frac{2\overline{U}_\theta}{R}\tilde{V} \tag{57}$$

$$S\tilde{V} = \left(DD_* - k^2\right)\tilde{V} - Re_\Omega\left(D_*\overline{U}_\theta\right)\tilde{U} \tag{58}$$

$$S\tilde{W} = -ik\tilde{P} + \left(D_*D - k^2\right)\tilde{W} \tag{59}$$

Here, the dimensionless variables and non-dimensional numbers are as follows. The outer radius r_2 is taken as the characteristic length

$$R=\frac{r}{r_2},\quad \overline{U}_\theta=\frac{\overline{u}_\theta}{\Omega_1 r_2},\quad \left(\tilde{U},\tilde{V},\tilde{W}\right)=\frac{(\tilde{u},\tilde{v},\tilde{w})}{\Omega_1 r_2},\quad \tilde{P}=\frac{\tilde{p}}{\rho\nu\Omega_1},$$
$$Re_\Omega=\frac{\Omega_1 r_2^2}{\nu},\quad k=r_2 a,\quad \eta=\frac{r_1}{r_2},\quad \mu=\frac{\Omega_2}{\Omega_1},\quad S=\frac{s}{\nu/{r_2}^2},\quad D=\frac{d}{dR},\quad D_*=\frac{d}{dR}+\frac{1}{R} \tag{60}$$

The boundary conditions are as follows:

$$\begin{cases} R=\eta: & \tilde{U}=\tilde{V}=\tilde{W}=0 \quad \text{(Inner wall)} \\ R=1: & \tilde{U}=\tilde{V}=\tilde{W}=0 \quad \text{(Outer wall)}. \end{cases} \tag{61}$$

After Chandrasekar [6], the following two non-dimensional numbers are introduced to verify the computational results:

$$Ta=\frac{4{\Omega_1}^2 r_1^4}{\nu^2}\frac{(1-\mu)(1-4\mu)}{(1-\eta^2)^2}=4{Re_\Omega}^2\frac{\eta^4(1-\mu)(1-4\mu)}{(1-\eta^2)^2},\quad \kappa=\frac{1-\mu/\eta^2}{1-\mu} \tag{62}$$

In this section, it is assumed that $S = 0$. This indicates that the secondary flow caused by the centrifugal instability is stationary and it contains toroidal vortices. To deal with the simultaneous ordinary differential equations for the boundary value problem, a one-dimensional staggered grid system is employed as shown in **Figure 5**. All the equations are discretized by the fourth order central difference method with a given wavenumber k using the HSMAC method [8] during which Re_Ω is obtained by the Newton method. The following equations are used for correction of the pressure and velocity simultaneously. Here, the subscript i indicates grid location, while the superscripts m and n indicate the iteration of the corrections for the convergence of Eq. (56) and the time step, respectively. The more detailed explanation can be found in the recent papers published by the present author [9, 10]

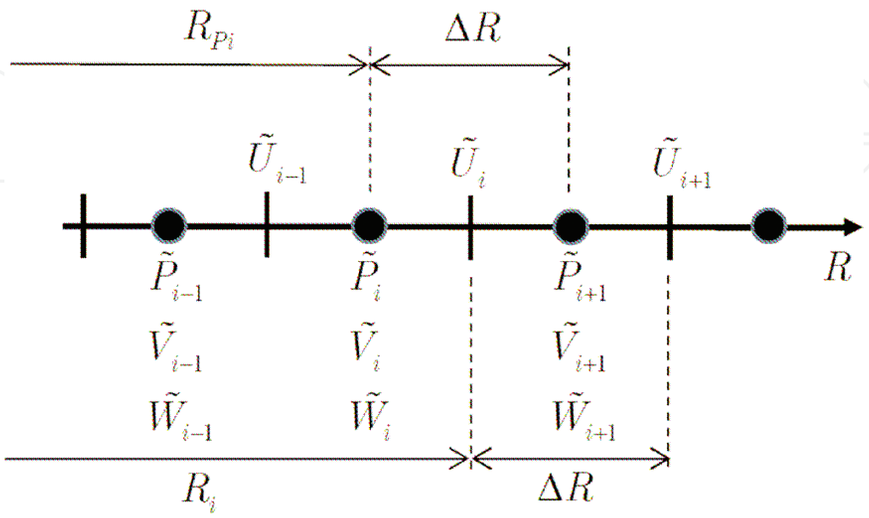

Figure 5. The staggered grids in the radius direction together with the points of each variable definition.

$$
\begin{aligned}
{}^{m+1}\tilde{P}_i^{n+1} &= {}^{m}\tilde{P}_i^{n+1} + {}^{m}(\delta\tilde{P})_i^{n+1} \\
&= {}^{m}\tilde{P}_i^{n+1} - \frac{\dfrac{-{}^{m}\tilde{U}_{i+1}^{n+1} + 27{}^{m}\tilde{U}_i^{n+1} - 27{}^{m}\tilde{U}_{i-1}^{n+1} + {}^{m}\tilde{U}_{i-2}^{n+1}}{24(\Delta R)} + \dfrac{-{}^{m}\tilde{U}_{i+1}^{n+1} + 9{}^{m}\tilde{U}_i^{n+1} + 9{}^{m}\tilde{U}_{i-1}^{n+1} - {}^{m}\tilde{U}_{i-2}^{n+1}}{16R_{Pi}} + ik\cdot{}^{m}\tilde{W}_i^{n+1}}{\Delta\tau\{2/(\Delta R)^2 + k^2\}}
\end{aligned}
\tag{63}
$$

$$
{}^{m+1}\tilde{U}_i^{n+1} = {}^{m}\tilde{U}_i^{n+1} + \frac{\Delta\tau}{\Delta R}\cdot{}^{m}\left(\delta\tilde{P}\right)_i^{n+1}, \quad {}^{m+1}\tilde{U}_{i-1}^{n+1} = {}^{m}\tilde{U}_{i-1}^{n+1} - \frac{\Delta\tau}{\Delta R}\cdot{}^{m}\left(\delta\tilde{P}\right)_i^{n+1} \tag{64}
$$

$$
{}^{m+1}\tilde{W}_i^{n+1} = {}^{m}\tilde{W}_i^{n+1} - ik(\Delta\tau)\cdot{}^{m}\left(\delta\tilde{P}\right)_i^{n+1} \tag{65}
$$

Table 2 shows the computational results for various rotation speeds at $\eta = 0.5$. When $\mu > 0.25$, the basic flow is always stable due to the Rayleigh's criterion. The present results exhibit slightly smaller values of Taylor number than those of Chandrasekar. **Figures 6** and **7** show the amplitude functions and Eigen functions, respectively, for the case of $\mu = 0$ (the outer cylinder is stationary), and **Figures 8** and **9** show the case of $\mu = -0.5$ (the outer cylinder rotates with half angular velocity in opposite direction to the inside rotation).

The simultaneous ordinary equations from (56) to (59) were divided into the real and imaginary parts. However, only four equations among the eight equations are necessary to solve in this problem because of the symmetricity and anti-symmetricity of the complex variables. In **Figures 6** and **8**, the real part of $\tilde{U}, \tilde{V}, \tilde{P}$ and the imaginary part of $\tilde{W}$ are shown. For the visualization shown in **Figures 7** and **9**, the Stokes stream function Ψ is defined as follows:

		Present (201 grids)		**Chandrasekar [6]**	
κ	μ	**Critical wave number**	**Critical *Ta* number**	**Wavenumber**	***Ta* number**
0	1/4	6.286	15316	6.4	15332
0.4	1/6	6.293	19518	6.4	19542
0.6	2/17	6.299	22617	6.4	22644
1.0	0	6.325	33062	6.4	33100
4/3	−1/8	6.403	53210	6.4	53280
1.6	−1/4	6.715	98520	6.4	99072
1.8	−4/11	7.819	197715	7.8	199540
1.9	−9/21	8.733	288761	8.6	293630
2.0	−1/2	9.602	417734	9.6	428650

Table 2. Computational results and comparison with Chandrasekar ($\eta = 0.5$).

http://dx.doi.org/10.5772/intechopen.72263

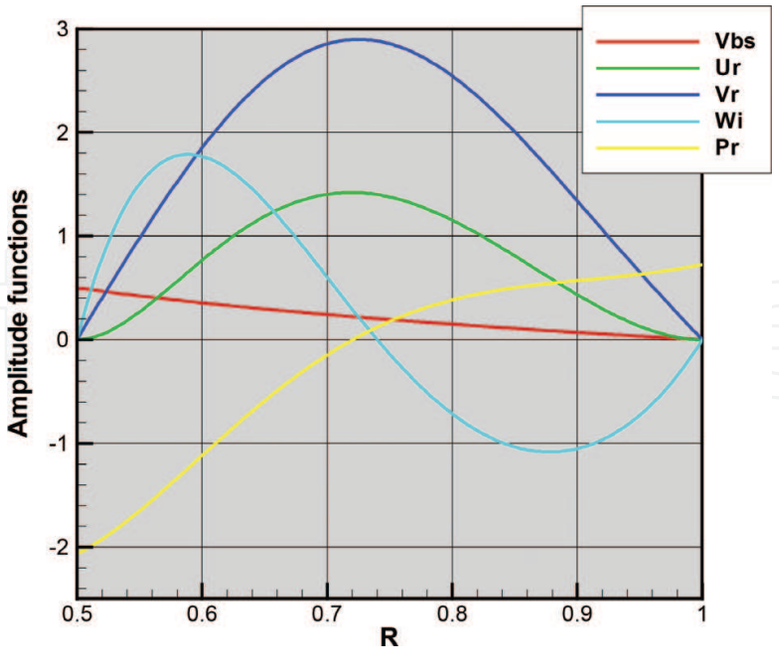

Figure 6. Amplitude functions ($\eta = 0.5$, $\mu = 0$, $k = 6.325$).

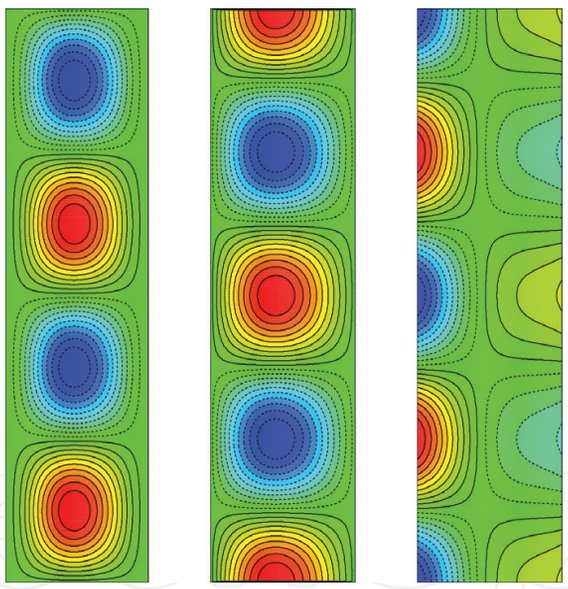

Figure 7. Visualization of Eigen functions for two wavelengths ($\eta = 0.5$, $\mu = 0$, $k = 6.325$). From left to right, Stokes stream function, azimuthal velocity, and pressure.

$$\tilde{U}_{\mathfrak{R}} \cdot \cos(kZ) = \frac{1}{R}\frac{\partial \Psi}{\partial Z}, \quad \tilde{W}_{\mathfrak{F}} \cdot \sin(kZ) = \frac{1}{R}\frac{\partial \Psi}{\partial R} \tag{66}$$

Here, the subscripts $\mathfrak{R}$ and $\mathfrak{F}$ represent the real part and the imaginary part, respectively. The visualization of other variables, such as the azimuthal velocity and the pressure, are treated in the similar manner using the trigonometric functions.

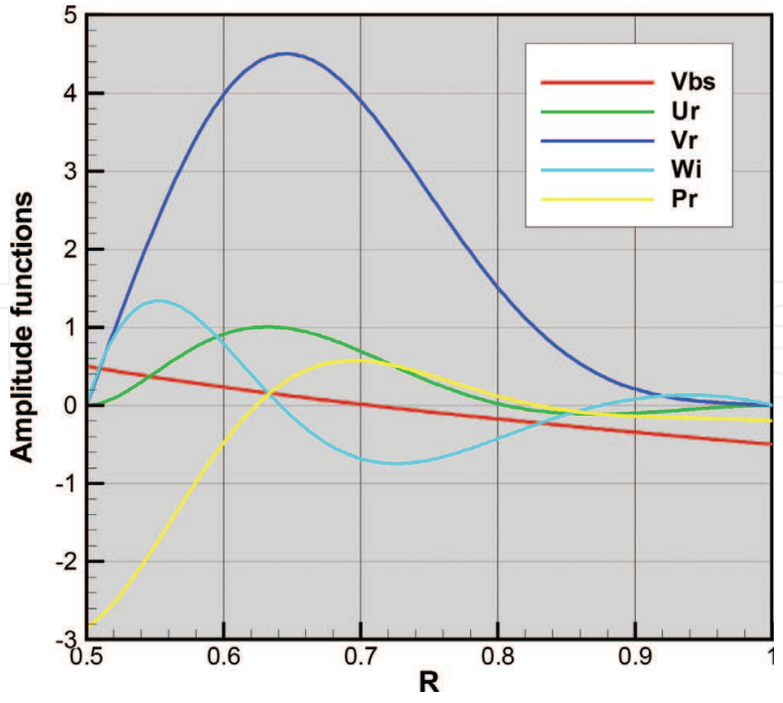

Figure 8. Amplitude functions ($\eta = 0.5$, $\mu = -0.5$, $k = 9.602$).

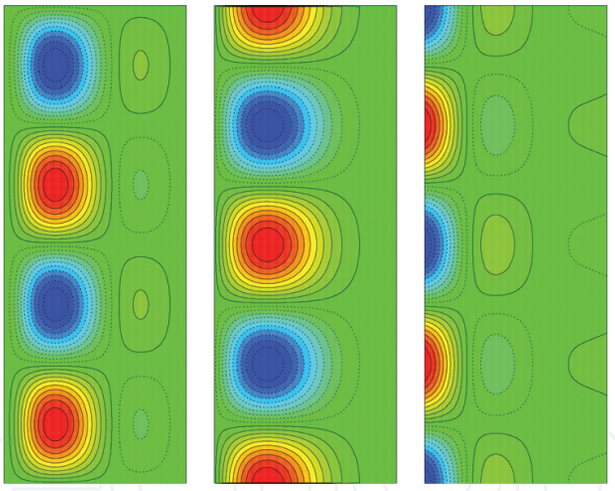

Figure 9. Visualization of Eigen functions for two wavelengths ($\eta = 0.5$, $\mu = -0.5$, $k = 9.602$). From left to right, Stokes stream function, azimuthal velocity, and pressure.

Author details

Toshio Tagawa

Address all correspondence to: tagawa-toshio@tmu.ac.jp

Department of Aerospace Engineering, Tokyo Metropolitan University, Japan

References

[1] Schlichting H, Gersten K. Boundary Layer Theory. 8th Revised and Enlarged ed. Berlin: Springer; 1999

[2] Stokes GG. On the effect of the internal friction of fluids on the motion of pendulums. Transactions of the Cambridge Philosophical Society. 1856;**9**(Part II):8-106 or Collected Papers III

[3] Rayleigh L. On the motion of solid bodies through viscous liquids. Philosophical Magazine. 1911;**21**:697-711

[4] Churchill SW, Ozoe H. A correlation for laminar free convection from a vertical plate. Journal of Heat Transfer. 1973;**95**(4):540-541

[5] Le Fevre EJ. Laminar free convection from a vertical plane surface. In: Proceedings of the 9th International Congress of Applied Mechanics; Brussels; Vol. 4; 1956. pp. 168-174

[6] Chandrasekar S. Hydrodynamic and Hydromagnetic Stability. Oxford: Clarendon Press; 1961

[7] Koschmieder EL. Bénard cells and Taylor vortices. In: Cambridge Monographs on Mechanics and Applied Mathematics. United State of America: Cambridge University Press; 1993

[8] Hirt CW, Nichols BD, Romero NC. SOLA: A Numerical Solution Algorithm for Transient Fluid Flows. Los Alamos, New Mexico, United State of America: Los Alamos Scientific Laboratory of University of California. 1975. p. LA-5852

[9] Tagawa T, Egashira R. Fluid flow of a liquid metal in a cylinder driven by a rotating magnetic field. Transactions of the Japan Society of Mechanical Engineers, Part B. 2012; **78**(794):1680-1695

[10] Tagawa T. Numerical investigation of Bénard-Marangoni convection of paramagnetic liquid in annular layers. In: The 15th International Heat Transfer Conference; Kyoto, Japan; August 2014

IntechOpen